Author Manuscript

Author Manuscript

Author Manuscript

Author Manuscript

HHS Public Access

Author manuscript

Neuron. Author manuscript; available in PMC 2017 December 21.

Published in final edited form as:

Neuron. 2016 December 21; 92(6): 1294–1307. doi:10.1016/j.neuron.2016.10.060.

The Mammalian Specific Protein Armcx1 Regulates Mitochondrial Transport During Axon Regeneration

Romain Cartoni[1,3], **Michael W. Norsworthy**[1], **Fengfeng Bei**[1], **Chen Wang**[1], **Siwei Li**[1], **Yiling Zhang**[1], **Christopher V. Gabel**[2], **Thomas L. Schwarz**[1,3], and **Zhigang He**[1,3,4]

[1]F.M. Kirby Neurobiology Center, Children's Hospital, and Department of Neurology, Harvard Medical School, 300 Longwood Avenue, Boston, MA 02115, USA

[2]Department of Physiology and Biophysics, Photonics Center, Boston University School of Medicine, Boston, Massachusetts 02118

Abstract

Mitochondrial transport is crucial for neuronal and axonal physiology. However, whether and how it impacts neuronal injury responses, such as neuronal survival and axon regeneration, remain largely unknown. In an established mouse model with robust axon regeneration, we show that Armcx1, a mammalian-specific gene encoding a mitochondria-localized protein, is up-regulated after axotomy in this high regeneration condition. Armcx1 overexpression enhances mitochondrial transport in adult retinal ganglion cells (RGCs). Importantly, Armcx1 also promotes both neuronal survival and axon regeneration after injury, and these effects depend on its mitochondrial localization. Furthermore, Armcx1 knockdown undermines both neuronal survival and axon regeneration in the high regenerative capacity model, further supporting a key role of Armcx1 in regulating neuronal injury responses in the adult central nervous system (CNS). Our findings suggest that Armcx1 controls mitochondrial transport during neuronal repair.

Introduction

After axotomy, a battery of alterations, such as membrane breakdown, cytoskeleton disassembly and calcium influx, occurs in injured axonal stumps. However, it remains poorly understood how injured neurons cope with such stresses and decide their survival and regenerative responses (Abe and Cavalli, 2008; Bradke et al., 2012; Goldberg and Barres, 2000; He and Jin, 2016). In intact conditions, neuronal mitochondria are transported along

[3]To whom correspondence should be addressed. zhigang.he@childrens.harvard.edu, thomas.schwarz@childrens.harvard.edu, romain.cartoni@childrens.harvard.edu.

[4]Lead contact

Publisher's Disclaimer: This is a PDF file of an unedited manuscript that has been accepted for publication. As a service to our customers we are providing this early version of the manuscript. The manuscript will undergo copyediting, typesetting, and review of the resulting proof before it is published in its final citable form. Please note that during the production process errors may be discovered which could affect the content, and all legal disclaimers that apply to the journal pertain.

Author Contributions

R.C. performed the experiments. R.C., T.L.S and Z.H. designed experiments and analyzed the data. M.W.N. provided technical assistance with RGCs survival and axonal regeneration experiments, C.W. performed optic nerve crush and AAV injections, F.F.B performed αRGCs experiments, S.L. provided technical assistance with the in situ hybridizations. C.V.G provided technical expertise on live imaging technique. R.C., T.L.S and Z.H wrote the paper.

Author Manuscript Author Manuscript Author Manuscript Author Manuscript

the axon across considerable distances to meet local needs for ATP and calcium buffering. Whereas mitochondria remain uniformly distributed along axons in non-growing conditions, mitochondrial distribution is biased towards the active growth cone when the axon is growing, suggesting that mitochondrial transport is regulated to support axonal growth (Morris and Hollenbeck, 1993). Thus, it is conceivable that mitochondrial dynamics might be important for regulating axonal and neuronal injury responses.

In all species, axonal mitochondria move bi-directionally along microtubule tracks. Their movement can be continuous or interrupted by pauses (for review see (Schwarz, 2013)). Previous studies revealed that an evolutionarily conserved protein complex that includes the mitochondrial GTPase Miro (also called RhoT1/2) and the adaptor Milton (also called Trak1/2) is essential for regulating the transport of mitochondria. However, considering the complexity of mitochondrial dynamics and its extensive regulation by signaling pathways (Courchet et al., 2013; Pekkurnaz et al., 2014; Wang et al., 2011), it is unknown what regulatory mechanisms might act in fine tuning mitochondrial transport during pathological conditions, such as after an injury.

In injured axons of the peripheral nervous system (PNS), it has been shown that regenerating axons increase mitochondrial movement (Mar et al., 2014; Misgeld et al., 2007), but the mechanisms underlying this response remain unclear. In addition, as most injured axons in the adult CNS cannot regenerate spontaneously, the regulation of mitochondrial transport and its relevance to axon regeneration in these axons has not been formally investigated. Therefore, whether increasing mitochondrial movement could have an impact on neuronal survival and axon regeneration remains an open question. In investigating the intrinsic regenerative ability of neurons, recent studies have led to the discovery of a number of molecules and pathways important for axon regeneration (reviewed by (Bradke et al., 2012; Cregg et al., 2014; Hammarlund and Jin, 2014; Lu et al., 2014). Manipulating these molecules, alone or in combination, resulted in significant axon regeneration in the adult CNS. For example, we have previously shown that robust and sustained axon regeneration in adult RGCs can be induced by deletion of PTEN, SOCS3 and/or by manipulating the c-Myc pathway (Belin et al., 2015; Park et al., 2008; Smith et al., 2009; Sun et al., 2012).

We reasoned that these mouse models with high regenerative capacity might provide useful tools to address the possible role of mitochondrial transport in axon regeneration and neuronal survivals in the CNS. Therefore, we used RGCs with high regenerative capacity induced by co-deletion of PTEN and SOCS3 (dKO). Among the highly up-regulated genes in this established mutant of high regeneration, we identified the Armadillo Repeat Containing, X-Linked 1 (Armcx1) gene, a member of a poorly characterized cluster of six genes unique to placental mammals (López-Doménech et al., 2012). We showed that Armcx1 localized to mitochondria and that its overexpression enhanced mitochondrial transport as well as promoted axon regeneration and neuronal survival *in vivo* .In contrast, Armcx1 down-regulation decreased the regeneration capacity of the dKO model. We further showed that the effects of Armcx1 on neuronal survival and axon regeneration were dependent on its mitochondrial localization. Together these findings demonstrate that Armcx1 is a mitochondrial transport regulator relevant for neuronal repair. We conclude that

Author Manuscript Author Manuscript Author Manuscript Author Manuscript

modulating mitochondrial transport after axonal injury might constitute a new strategy to counteract neuronal cell death and the lack of axonal regeneration ability.

Results

Armcx1 expression is up-regulated in RGCs with high regenerative capacity

Because of the essential role of mitochondria in axonal physiology, using a loss of function approach to determine how regulators of mitochondrial dynamics influence axon regeneration might be difficult to interpret. Instead, we reasoned that neurons characterized by a high regenerative capacity after axonal injury would constitute an ideal starting point to identify mitochondrial transport regulators involved in axon regeneration. In our previous studies (Sun et al., 2012), we compared gene expression profiles in injured RGCs with poor regenerative ability (wild type mice) and with induced high regenerative ability, referred to in this paper as the dKO model ($PTEN^{f/f}$;$SOCS3^{f/f}$ mice with vitreous injection of AAVs expressing Cre (AAV-Cre) and CNTF (AAV-CNTF), CNTF being used to further elevate the Jak/STAT signaling after SOCS3 deletion, Smith et al., 2009; Sun et al., 2012). From these datasets, we did not find any genes that have previously been implicated in mitochondrial transport, such as Milton or Miro, to be differentially expressed in these neurons with different regenerative ability. However, Armcx1, a member of a cluster of genes in which a family member, Armcx3, had been implicated in regulating mitochondrial transport (López-Doménech et al., 2012), appeared to be highly expressed in injured RGCs with induced regenerative ability (Sun et al., 2012).

We first verified the expression of Armcx1 and its paralogs in RGCs by *in situ* hybridization. As shown in Figure 1A, low levels of Armcx1 signal were detected in some RGCs of wild type mice, which were not affected by injury. In stark contrast, 3 days after injury, Armcx1 signal was significantly increased in the RGCs of the $PTEN^{f/f}$;$SOCS3^{f/f}$ mice with vitreous injection of AAV-Cre and CNTF (dKO), but not of $PTEN^{f/f}$ mice with vitreous injection of AAV-Cre ($PTEN^{-/-}$), consistent with the gene profiling results (Sun et al., 2012). In comparison, other Armcx members, including 3, 5, and 6, were expressed at low levels in all conditions (Figure S1A). The up-regulation of Armcx1 in dKO injured RGCs was further supported by immunohistochemistry (Figure 1B and 1C), which showed that RGCs positively stained with anti-Armcx1 increased approximately two-fold in the dKO after injury compared to other conditions (Figure 1C; 40% in injured dKO compared to 20% in other conditions). Based on these results, we decided to focus on Armcx1 for our further studies.

Armcx1 localizes to mitochondria and interacts with mitochondrial transport machinery

Similar to other members of the Armcx cluster, Armcx1 has a putative mitochondrial outer membrane-targeting sequence flanking the trans-membrane (TM) domain (Figure 1D) (Mou et al., 2009). We designed a mutant of Armcx1 that lacks its transmembrane domain, Armcx1ΔTM (Figure 1D and 1E) and assessed the localization of Armcx1 and Armcx1ΔTM by co-transfecting HA-tagged Armcx1 or Armcx1ΔTM with the mitochondrial marker MitoDsRed in mouse cortical neurons. We showed that the vast majority of Armcx1 protein

Author Manuscript Author Manuscript Author Manuscript Author Manuscript

was targeted to mitochondria (Figure 1F and Figure S1B), while the absence of the TM domain of Armcx1 prevented its mitochondrial localization (Figure 1G and Figure S1B).

Armcx3 was recently shown to regulate mitochondrial transport by interacting with the mitochondria trafficking regulatory complex that connects mitochondria to the motor proteins (López-Doménech et al., 2012), which prompted us to test whether Armcx1 has similar capacities. Co-immunoprecipitation using Armcx1-HA and Miro1-Myc showed that Armcx1 interacted with Miro1 (Figure 1H), the protein linking mitochondria to the Trak1-Kinesin motor complex. Together, these results indicate that the mitochondria-localized Armcx1 protein is up-regulated in RGCs with induced regenerative ability and suggest that Armcx1 might be a candidate in regulating mitochondrial trafficking.

Armcx1 overexpression enhances mitochondrial transport in adult RGC axons—Axonal mitochondria are distributed in two pools: the motile pool, which can move bidirectionally and may pause before resuming movement, and the stationary pool, which is fixed in position typically for the observable duration of an experiment. The proportion of these two pools has been suggested as an important indicator of mitochondrial trafficking in axons (Schwarz, 2013). As a first step to assess the role of Armcx1 in the injury responses of adult RGCs, we examined whether enhancing the expression of Armcx1 would increase mitochondrial transport in adult RGC axons using retina explant cultures coupled with live imaging microscopy. Because of the poor neuronal survival and neurite growth of adult wild type retinal explants, we took advantage of the $PTEN^{-/-}$ mice whose RGCs showed better survival and axonal outgrowth in explant cultures (Nawabi et al., 2015). Since PTEN deletion alone did not significantly increase Armcx1 levels (Figure 1A), this mutant is suitable for assessing the effects of overexpressed Armcx1. $PTEN^{f/f}$ adult mice were intravitreally injected with AAV-Cre and AAVs expressing either full length Armcx1 or the Armcx1ΔTM mutant. As a control, we used AAV expressing placental alkaline phosphatase (PLAP), a well-established non-fluorescent and inert control for viral injection (Bei et al.; Belin et al., 2015; Nawabi et al., 2015). Immunohistochemistry on whole mount retina confirmed the efficient infection of RGCs by AAVs encoding Armcx1 full length and mutant (Figure S2A and S2B). To confirm that multiple viral co-injections allowed efficient targeting of RGCs in explant culture, we co-injected AAV expressing a mitochondrial protein (Cre-dependent MitoDsRed; AAV2-FLEX-MitoDsRed) with AAV-Cre to the vitreous body of $PTEN^{f/f}$ mice and showed that the vast majority of the neurites growing out of the resultant explants were MitoDsRed positive (Figure S2C).

The proportion of motile versus stationary mitochondria in axons overexpressing Armcx1 was assessed using live recording of mitochondrial transport. Unlike dissociated neuronal culture in which the morphology of mitochondria in the soma is used to confirm neuronal health prior to imaging, explant culture does not allow access to RGC cell bodies. To circumvent this issue, we used mitochondrial membrane potential as a marker of axonal health by labeling mitochondria with tetramethylrhodamine methyl ester (TMRM), a membrane potential dependent fluorescent dye (Trushina et al., 2012; Verburg and Hollenbeck, 2008; Zhang et al., 2016). We found that Armcx1 overexpression induced a significant increase of the motile mitochondria pool compared to the PLAP control (Figure 2A and 2B and Movie S1). In contrast, the mutant Armcx1ΔTM failed to do so (Figure 2A,

Author Manuscript Author Manuscript Author Manuscript Author Manuscript

2B), suggesting that the effect of Armcx1 on mitochondrial motility is dependent on its mitochondrial localization. Consistent with the increase of the motile mitochondrial pool, Armcx1 overexpression increased the moving frequency of the total pool of mitochondria, i.e. the fraction of time mitochondria in motion rather than paused (Figure 2C). To further determine whether the overexpression of Armcx1 increased the transport of mitochondria from the motile pool, we specifically analyzed the moving frequency of this pool and did not observe any difference between control and Armcx1 overexpression (Figure S2D). Since Armcx1 overexpression increased the proportion of motile mitochondria with no accompanying changes of mitochondrial density (Figure 2D), we concluded that Armcx1 likely increases mitochondrial transport by recruiting stationary mitochondria into the motile pool.

Armcx1 promotes retinal neurite outgrowth—In addition to mitochondrial movement, we also assessed the effects of Armcx1 on neurite outgrowth from these retinal explants. Immunohistochemistry against the neuronal marker Tuj1 revealed that Armcx1 overexpression triggered a substantial increase in axons growing out of the explants (Figure 2E-G) independent of their size (Figure 2F). Detailed analysis showed that the Armcx1-induced axonal outgrowth was more evident at short distances (Figure 2E lower panel and 2G). Consistent with the mitochondrial transport data, the overexpression of the non-mitochondrial Armcx1 mutant (Armcx1ΔTM) failed to reproduce the outgrowth phenotype observed with full length Armcx1 (Figure 2E-G), suggesting a direct link between Armcx1 localization on mitochondria and enhanced axonal outgrowth.

Armcx1 regulates mitochondrial transport and neurite outgrowth in embryonic neurons—In order to test whether Armcx1 overexpression has a general effect on mitochondrial transport and neurite outgrowth, we performed similar analyses as described above in cultured E18 cortical neurons, a well-established system for investigating mitochondrial trafficking (Pekkurnaz et al., 2014; Wang and Schwarz, 2009; Wang et al., 2011). We first asked whether Armcx1 overexpression could alter the proportion of motile versus stationary mitochondria in these neurons. We therefore co-transfected the mitochondrial marker MitoDsRed with either Armcx1 or GFP as a control. Armcx1 expression was coupled with a GFP reporter linked by an F2A sequence allowing the identification of transfected neurons. Whereas in wild type axons around 50% of mitochondria were motile, Armcx1 overexpression significantly increased the percentage of motile mitochondria up to 80% (Figure 3A and 3B, Movie S2). Consistently, Armcx1 overexpression also significantly increased the moving frequency of mitochondria (Figure 3C) with no effect on mitochondrial density (Figure S3A). In contrast to its effect on mitochondria trafficking, overexpressing Armcx1 did not affect the transport of BDNF positive vesicles (Figure S3B and S3C), consistent with a specific localization of Armcx1 to mitochondria. In addition, Armcx1 overexpression significantly increased the average length of the longest neurites of embryonic cortical neurons (Figure 3D and 3E). These results together suggest that Armcx1 overexpression leads to similar effects on enhancing mitochondria movement and neurite growth in both adult RGC axons and embryonic cortical neurons.

Author Manuscript Author Manuscript Author Manuscript Author Manuscript

Armcx1 promotes neuronal survival and axon regeneration after optic nerve injury—The above results suggest that Armcx1 might have a role in promoting neurite outgrowth. We hypothesized that this role could be important to promote axonal regeneration after an injury. To directly test this hypothesis, we examined the effects of Armcx1 overexpression on axon regeneration and neuronal survival in adult RGCs after an optic nerve crush injury. AAVs encoding Armcx1, Armcx1ΔTM or PLAP were injected into the vitreous body of adult wild type mice and optic nerve crush was performed one month after viral injection. 15 days after injury, the regenerating axons were labeled with the anterograde tracer CTB. We found that Armcx1 overexpression induced a significantly higher number of regenerating axons in comparison to PLAP control (Figure 4A-C). Consistent with in vitro data, this effect was dependent on Armcx1 mitochondrial localization since the overexpression of Armcx1ΔTM failed to recapitulate the enhanced regeneration (Figure 4A-C). Furthermore, we also analyzed the effect of Armcx1 overexpression on the survival of RGCs (Figure 4D and 4E). Consistent with our previous studies (Belin et al., 2015; Nawabi et al., 2015; Park et al., 2008; Smith et al., 2009), about 25% of RGCs survived in the control group (Figure 4D and 4E). Strikingly, overexpressing Armcx1, but not the non-mitochondrial mutant Armcx1ΔTM, led to an increase of approximatively 45% of neuronal survival compared to the control group (Figure 4D and 4E), suggesting that Armcx1 may not only promote axon regeneration but also protect injured neurons from cell death.

In principle, the observed regenerative effects of Armcx1 overexpression might reflect a direct effect of Armcx1 on axon regeneration or be merely secondary to increased neuronal survival. Several strategies such as p53 deletion (Park et al., 2008), manipulating ER stress pathways (Hu et al., 2012), and Apaf1-deleted mice (unpublished data), are able to increase neuronal survival but not axon regeneration in the same optic nerve injury model, suggesting that axon regeneration requires an independent mechanism. To directly test this in the context of Armcx1, we took advantage of a transgenic mouse line in which Bcl-2 is overexpressed under a pan neuronal promoter (Martinou et al., 1994). Consistent with previous results using Bcl-2 transgenic mice (Bei et al.; Bonfanti et al., 1996; Goldberg et al., 2002), about 80% of RGCs survived but no significant increase in axon regeneration occurred 2 weeks after injury (Figure S4). With Armcx1 overexpression, high neuronal survival remained at 15 days after injury in these mice (Figure S4A and S4B). Importantly, even with this high survival rate, Armcx1 overexpression improved axon regeneration of Bcl-2 mice (Figure S4C and S4D) but did not further enhance the extent of axon regeneration beyond what was observed by Armcx1 overexpression in the absence of Bcl-2 (Figure S4C and S4D compare to the results in Figure 4A-C). Therefore, these findings substantiate the notion that, in addition to promoting neuronal survival, Armcx1 is also directly involved in regulating the process of axon regeneration after injury.

Armcx1 potentiates the regeneration of PTEN deleted RGCs—Although Armcx1 has a positive effect on axon regeneration in wild type mice, the limited numbers of regenerating axons might reflect compromised regenerative ability associated with injured RGCs. As our previous studies showed that PTEN deletion in adult RGCs is able to increase neuronal survival and axon regeneration by elevating mTOR activity in injured RGCs (Park

Author Manuscript Author Manuscript Author Manuscript Author Manuscript

et al., 2008), we tested the effect of Armcx1 in this regeneration-permissive background. AAVs expressing Cre together with AAVs expressing Armcx1, Armcx1ΔTM or PLAP as a control, were co-injected to the vitreous body of adult $PTEN^{f/f}$ mice and optic nerve crush was performed 4 weeks after viral injection. After an additional 15 days, the regenerating fibers were labeled with the anterograde tracer CTB and examined in optic nerve cross-sections. We found that in this PTEN-deleted background, Armcx1 overexpression induced a significant increase in the number of regenerating axons in comparison with PTEN deletion alone (Figure 5A and 5B and S5A). This increase is most striking for the short-regenerating axons, consistent with the results of neurite outgrowth in retinal explants (Figure 2E-G). We further showed in a side-by-side study that the high regeneration capacity of PTEN deleted RGCs overexpressing Armcx1 fell within the same range as the dKO phenotype (Figure S5B and S5C). In addition, Armcx1 overexpression also further increased RGC survival induced by PTEN deletion (Figure 5C and 5D). As expected, the mutant Armcx1ΔTM failed to alter either neuronal survival or axon regeneration (Figure 5A-5D).

Previous studies demonstrated that among different RGC subtypes analyzed, PTEN inhibition selectively promotes regeneration from αRGCs (Duan et al., 2015). The high number of injured axons growing beyond the injury site when Armcx1 was overexpressed in PTEN deleted mice (Figure 5A and 5B) prompted us to test the effects of Armcx1 on promoting the regeneration of different RGC subtypes. To this end, we used the mouse line Kcng4-Cre; Thy1-stop-YFP line 1 (Kcng4-YFP) that labels αRGCs and their axons (Duan et al., 2015; 2014). To inhibit PTEN expression, we injected AAVs expressing shRNA against PTEN (Duan et al., 2015; Zukor et al., 2013) with or without AAV-Armcx1 to the Kcng4-YFP mice. At 15 days post injury, CTB injection was performed in order to label all regenerating axons from both αRGCs and non-αRGCs. Therefore, YFP+/CTB+ axons should be derived from αRGCs, while the YFP-/CTB+ axons are likely to be from non-αRGCs. As shown in Figure 5E and 5F, Armcx1 overexpression induced a significant increase in regenerating axons from non-αRGCs as quantified at 0.5 mm distal from the lesion sites. αRGC-derived regenerating axons also showed a trend of increase, but did not reach statistical significance (Figure 5F). These results suggest that in contrast to the selective effects of PTEN inhibition on αRGCs, Armcx1 is likely to promote axons regeneration from non-αRGCs and possibly from αRGCs to some extent.

Armcx1 knockdown reduces axon regeneration and neuronal survival in dKO mice—The positive effect of Armcx1 overexpression on axonal regeneration and neuronal survival led us to assess the functional outcomes of silencing Armcx1 expression in both in vitro and in vivo models. We tested five shRNAs targeting different regions of Armcx1 and found two with knockdown efficiency close to 80% (Figure S6A and S6B and data not shown). In order to maximize the knockdown efficiency we generated a vector harboring these two different shRNAs for the subsequent experiments (Song et al., 2008). We assessed the effects of Armcx1 knockdown on mitochondrial movement and other functional readouts in cultured E18 cortical neurons, by co-transfecting MitoDsRed with either shRNAs against Armcx1 or shRNA Scramble as a control. To facilitate the identification of transfected neurons these shRNA constructs were designed to carry a fluorescent protein reporter. Knockdown of Armcx1 had a significant effect on mitochondrial transport in axons,

Author Manuscript Author Manuscript Author Manuscript Author Manuscript

decreasing the motile pool from 60% to 20% (Figure S6C and S6D). Armcx1 silencing also significantly decreased the moving frequency of mitochondria (Figure S6E), without affecting mitochondrial density (Figure S6F). Importantly, knockdown of Armcx1 also significantly reduced neurite growth from transfected neurons (Figure S6G and S6H). Thus, these results are consistent with our overexpression data and support a role of Armcx1 in regulating mitochondria movement and neurite growth in cultured cortical neurons.

Finally, we tested whether the up-regulation of Armcx1 in RGCs of dKO mice is necessary for their high-regeneration phenotype. To directly test this hypothesis, we knocked down Armcx1 in dKO mice in which Armcx1 is up-regulated (Sun et al., 2012, Figure 1A-C). AAV carrying shRNAs against Armcx1 and the control shRNA Scramble were generated. These two viruses were both able to efficiently infect RGCs (Figure S6I). To assess the effects of shRNA Armcx1 virus on Armcx1 expression in injured dKO RGCs we injected AAV-Armcx1 shRNAs or Scramble in the retina of dKO mice. 5 weeks post injection of the shRNA AAVs, we performed optic nerve crush and terminated the animals 3 days post injury. Approximately 50% of RGCs were Armcx1 positive in dKO retinas with injection of AAV expressing shRNA-Scramble (Figure 6A), consistent with our immunohistochemistry results from Figure 1B and 1C. In contrast, AAV expressing Armcx1-shRNAs significantly reduced this number, bringing the percentage of Armcx1 positive RGCs to a level comparable to wild type condition, i.e. around 20% (Figure 6A).

To study the effect of Armcx1 down-regulation on axon regeneration in dKO mice, we used mice from the same cohort described above but terminated the mice 15 days post injury. As shown in figure 6B and Figure S6J, knocking down Armcx1 significantly inhibited the axon regeneration phenotype. Whole mount retina analysis revealed that shRNAs of Armcx1 also significantly reduced RGC survival in dKO mice, compared to the control Scramble shRNA (Figure 6C). In a separate control, we injected the same AAV vectors to the vitreous bodies of wild type mice and analyzed these mice at 5 weeks post injection. CTB traced optic nerve axons did not show any sign of degeneration comparing to control injected with AAV-shRNA Scramble and RGC survival was not significantly different between conditions (Figure S6K). Together, these results suggest that injury-induced Armcx1 expression is required for the increased neuronal survival and axon regeneration phenotypes of the dKO model.

Discussion

In this study, we show that the mitochondrial protein Armcx1 is sufficient to (1) increase mitochondrial transport by recruiting stationary mitochondria, (2) protect axotomized neurons from cell death, and (3) promote axon regeneration. We further show that Armcx1 is necessary for the axon regeneration and neuronal survival phenotypes observed in high regenerative conditions induced by the co-deletion of PTEN and SOCS3 and an accompanying treatment of CNTF (dKO). Together with the fact that Armcx1 expression is injury-induced and correlates with high regenerative ability, our results suggest Armcx1 as a key regulator of mitochondrial transport in injured axons, which could impact neuronal survival and axon regeneration. We propose that modulated mitochondrial transport might constitute a new strategy to promote neuronal repair of the injured CNS.

Author Manuscript Author Manuscript Author Manuscript Author Manuscript

The precise mechanisms of Armcx1 in injured axons remain to be determined. Similar to Armcx3, Armcx1 is able to interact with the Miro/Trak mitochondrial transport complex. However, it remains to be determined whether Armcx1 mobilizes stationary mitochondria in a calcium dependent manner as has been proposed for Armcx3 (López-Doménech et al., 2012). Like other members of the Armcx cluster, Armcx1 has a nuclear localization signal (Figure 1D and (López-Doménech et al., 2012)). In our studies, we also found that some overexpressed Armcx1 is localized to the nuclei of transfected neurons (data not shown). Thus, although we cannot rule out other functions of Armcx1, the results from the Armcx1ΔTM mutant suggest that the mitochondria-targeted Armcx1 protein is responsible for its function in promoting axon regeneration and RGC survival. In the same line, a recent study showed that enhancing mitochondrial transport by genetic deletion of the gene encoding the mitochondria-anchoring protein syntaphilin also facilitated axon regeneration by rescuing energy deficits in injured axons (Zhou et al., 2016). However, whether Armcx1 acts by regulating energy supply or other mechanisms, such as regulation of calcium homeostasis, signaling via reactive oxygen species, or changes in the production of metabolites, requires further studies. In addition, sustained axon regeneration likely involves the enhanced axonal transport of not only mitochondria but also other axonal building blocks. Thus, it would be interesting to identify other regulators of axonal transport in neurons with increased regenerative ability.

In the PTEN deletion background, Armcx1 overexpression further increased the number of regenerating axons (Figure 5A, B and S5). Interestingly, this is in contrast with other treatments, such as overexpression of DCLK2, a cytoskeleton regulator, which increases the length of regenerating axons without substantially affecting the number of regenerating axons induced by PTEN deletion (Nawabi et al., 2015). These results, together with our loss of function experiment where Armcx1 down-regulation inhibited dKO-induced axon regeneration (Figure 6), suggest that Armcx1 is more important for the initiation phase of axon regeneration. The increased regeneration observed with Armcx1 overexpression is unlikely to be merely secondary to improved neuronal survival because RGC loss is efficiently prevented by Bcl-2 expression, although Bcl-2 does not increase regeneration. Moreover, in the Bcl-2 expressing background Armcx1 enhances regeneration without an additive effect on RGC survival (Figure S4). Finally, even though expression of Armcx1 shRNA reduced RGC regeneration in dKO mice back to a level comparable to wild type mice (Figure 6B and Figure 4A), RGCs survival was less drastically affected (Figure 6C and Figure 4E).

We showed that in a PTEN deletion background, Armcx1 overexpression facilitates additional axon regeneration from non-αRGCs, a cell type that otherwise exhibits little regeneration. It is possible that different RGC sub-types have different needs in terms of mitochondrial function; non-αRGCs may have a greater dependency on mobilization of mitochondria by Armcx1 in order to cope with injury-induced stresses such as calcium influx and energy imbalance. However, it is unknown whether Armcx1 effects somatic mitochondria the same as axonal mitochondria; these differentially localized mitochondria may be responsible for distinct effects on neuronal survival and axon regeneration. Nevertheless, as visual functions appear to be executed by different classes of RGCs (Sanes

Author Manuscript Author Manuscript Author Manuscript Author Manuscript

and Masland, 2015; Wernet et al., 2014), these results might be insightful for designing more efficient neural repair strategies to target different populations of RGCs.

The Armcx-cluster specificity to Eutherian mammals might imply that it has evolved as an additional layer of mitochondrial transport regulation to match the increasing complexity of the mammalian CNS. Our results suggest that this extra layer of regulation might be especially important when stress, such as an injury, is applied to the axon. Because mitochondrial transport failure has been reported in many neurodegenerative diseases (De Vos et al., 2008), increasing mitochondrial transport has been proposed as an exciting option to counteract axonal degeneration and subsequent neuronal death (Hinckelmann et al., 2013). With this perspective, the present study suggests that Armcx1 and its homologues could be a set of important targets of therapeutic interventions for neuronal protection and repair.

Experimental procedure

Mouse Strains

PTEN$^{f/f}$; SOCS3$^{f/f}$ mice were obtained by breeding PTEN$^{f/f}$ (Park et al., 2008) and SOCS3$^{f/f}$ (Smith et al., 2009). Kcng4-cre; Thy1-stop-YFP line was a kind gift from Josh Sanes laboratory (Duan et al., 2015). For Bcl-2 experiments, because of mouse strain availability we used the Bcl-2/PTEN$^{f/f}$/SOCS3$^{f/f}$ line (Bei et al. 2016). Without expressing the Cre recombinase this line show no axon regeneration ((Bei et al. 2016) and Figure S4D) and is considered as base line controls. Throughout all paper dKO conditions used as a model of high regeneration refers to PTEN$^{f/f}$; SOCS3$^{f/f}$ mice +AAV Cre +AAV CNTF (Sun et al., 2012). CNTF is used to potentiate the effect of SOCS3 deletion alone (Smith et al., 2009).

Constructs

The Armcx1-HA, Armcx1ΔTM-HA, PLAP and Armcx1F2AGFP vectors were generated from the pAAV-MCS constructs (Stratagene). For shRNA Armcx1 constructs, two targeting sequences against Armcx1 (shRNA2; targeting sequence GAGAGGCAAACCTCAAGATGACTC and shRNA5; TCAGTCAAGTGTGTGACGATACC were cloned into pAAV-Armcx1-2in-shRNA-mCherry vector from ViGene Biosciences. The construct was generated by ViGene Sciences, Inc. Control shRNA Scramble construct was generated from the pAAV-U6-GFP (Cellbiolabs).

Retina Explant culture

P21 PTEN$^{f/f}$ mice were injected with AAV2-Cre and AAV2-PLAP (placental phosphatase alkaline) as control, AAV2-Armcx1HA or AAV2-Armcx1HAΔTM. 2 weeks after, retinas were dissected out in Hibernate-A (Brain Bits). Retina explants were then plated onto Poly-L-Lysin (Sigma) and Laminin (Sigma) coated glass bottom dishes (MatTek) in Neurobasal-A (Life Technology) supplemented with B-27 (Life Technology), L-Glutamine (Life Technology) and Penicillin/Streptomycin (Life Technology). To evaluate axonal outgrowth, explants were fixed in PFA 4%/Sucrose 1,5% in PBS after 2 weeks and labeled with primary

Author Manuscript Author Manuscript Author Manuscript Author Manuscript

antibody anti-Tuj1 (Covance Research Products Inc Cat# MMS-435P, RRID:AB_2313773 or Covance Research Products Inc Cat# MRB-435P-100, RRID:AB_10175616), secondary antibody Alexa-488 (1/400-Life Technology). For live imaging experiments, explant were incubated with tetramethylrhodamine methyl ester (TMRM) (Life Technologies) as described in (Verburg and Hollenbeck, 2008).

In situ hybridization and Immunohistochemistry

Animals were perfused intracardially with PBS followed by paraformaldehyde (PFA-Sigma) 4% in PBS (w/v). After dissection, tissues were post fixed in PFA 4% in PBS overnight at 4°C and then incubated in Sucrose (Sigma) 15% in PBS for 48h at 4°C. Samples were embedded in Tissu-Tek and frozen at −80°C. Eyes were sectioned by cryostat at 20um. In situ hybridization was performed following classical protocol as described in (Nawabi et al., 2010). For Immunohistochemistry of whole mount retina, retinas from perfused animals were washed in PBS and blocked in 96 wells plates with PBS-Triton 0.3%-BSA 2% during one hour. Antibodies against HA (Roche Cat# 11867431001, RRID:AB_390919) and Tuj1 (Covance Research Products Inc Cat# MRB-435P-100, RRID:AB_10175616) were apply on retina in blocking buffer and apply on retina overnight at 4°C. After PBS wash, retinas were incubated for a minimum of 2 hours at room temperature with Alexa secondary antibodies, washed with PBS and mount with fluoromount (SouthernBiotech). Retinas cross sections for immunohistochemistry study of Armcx1 was prepared as described above. Immunohistochemistry using Armcx1 antibody (Abcam Cat# ab65144, RRID:AB_1141088) was performed using Tyramide Signal Amplification system (TSA, Perkin Elmer) following manufacturer protocol. Tuj1 positive RGCs (Covance Research Products Inc Cat# MMS-435P, RRID:AB_2313773) were determined positive for Armcx1 when signal intensity was minimum 60% above background.

Cortical neurons culture and transfection

Cortical neurons were isolated from E18 mouse embryo (Charles River). Briefly, cortices were chemically dissociated in papain solution (Worthington Biochemicals) for 10mn at 37°C followed by two wash in trypsin inhibition solution (Sigma T9253) and mechanical dissociation using P1000 plastic tip in plain Neurobasal medium (Life Technology). Dissection, dissociation and wash were done in HBSS (Gibco 1470-112) with 45% glucose and kynurenic acid (Sigma K3375) solution (HBSS, kyuneric acid 10mM, 100mM Hepes, 100mM MgCl2). Cells were plated on poly-l-lysine hydrobromide (Sigma) coated 35mm glass bottom dish (MatTek, (90’000 cells/wells). Neurons were cultured in Neurobasal medium (Life Technology) supplemented with B-27 (Life Technology), L-Glutamine (Life Technology) and Penicillin/Streptomycin (Life Technology). Half of the medium was replaced every other day. Plasmid DNA transfections were performed using Lipofectamin 2000 (Invitrogen) following manufacturer procedure. We used 0.3μg of vector GFP, AAV-Armcx1F2AGFP, MitoDsred2 (Promega) and 0.5 μg of shRNA plasmids. To study mitochondrial and BDNF positive vesicles transport neurons were transfected at DIV 5. At DIV7 the culture medium was replaced by Hibernate E low fluorescence (BrainBites) to maintain cell viability in CO2-free conditions during live imaging. For neurites outgrowth experiments, neurons were transfected at DIV1.

Author Manuscript Author Manuscript Author Manuscript Author Manuscript

Cortical Neurons Immunohistochemistry

For immunohistochemistry of cortical neurons, DIV 5-7 neurons were fixed with 4% PFA/ 1.5% Sucrose in PBS and immunostained using standard procedure (Glater et al., 2006). Briefly, fixed neurons in glass bottom dish were incubated for 5mn in PBS-Triton 0.3% followed by 1 hour in blocking solution (NGS 10%, Triton 0.1% in PBS). Primary antibodies against HA (Roche Cat# 11867431001, RRID:AB_390919), GFP (Abcam Cat# ab13970, RRID:AB_300798) or RFP (Abcam Cat# ab62341, RRID:AB_945213) were incubated overnight. After PBS wash, secondary anti-rat antibody (1/400, Life Technologies) was added for 1 hour. Cover slips were mounted using Fuoromount-G (SouthernBiotech).

Protein analyses and Co-immunoprecipitation

For Western blot analyzing of Armcx1 constructs, proteins were extracted from Lipofectamin transfected HEK cells (0.5μg of DNA) and immunoblot was performed as described in (Cartoni et al., 2005) with minor modifications. Co-immunoprecipation was performed as described in (López-Doménech et al., 2012). Briefly, HEK cells were transfected with 2.5μg of each plasmid. 3 days later, cells were lysed in lysis buffer (Tris-HCl pH: 7.5, NaCl 150mM, MgCl2 1.5mM, EDTA 5mM Triton 1%, Glycerol 10% and protease inhibitor cocktail). Immunoprecipitation was performed using Dynabeads Protein G (Novex 10003D) and following manufacturer protocol including mixing beads with 20μg of antibody (Roche Cat# 11867431001, RRID:AB_390919) for 10mn on wheels at room temperature and a 1 hour incubation at room temperature with the cell homogenate. For elution a wash buffer was used (TrisHCl pH: 8, NaCl 500mM, EDTA 1mM, EGTA 1mM, Triton 1%, NP-40 0.5%).

Live imaging

Adult retina explants—Time-lapse movies were acquired on a PerkinElmer Spinning Disc confocal microscope equipped with a temperature-controlled chamber at 37°C and with a 20 × oil objective. Each frame was captured every 2s. and 60 frames were acquired in total for each recording with laser power set to 30% for each channel to minimize damage. A portion of 80-120 μm of axon located 150μm from the tip was selected for analysis. Volocity software (PerkinElmer) was used for live recording. For both the retina explant and the cortical neuron images, we used a custom-made Image J macro for kymograph based motility analysis as described in (Pekkurnaz et al., 2014). Image J raw data were extracted as excel spreadsheets (Microsoft Excel) and statistical analysis was performed with GraphPad Prism version 6.0 for Mac OS X (GraphPad Software, Inc., La Jolla, CA, USA). E18 cortical neurons. Neurons were transferred into pre-warmed Hibernate medium without phenol red, which buffers CO_2 (Brain Bits). Transfected axons were detected using the GFP channel. Single axons were imaged on an inverted Nikon Eclipse Ti-U microscope and 1 frame was captured every 2s. 60 frames were acquired in total for each recording.

Mitochondrial transport analysis

From the kymograph generated by the live imaging files, mitochondrial transport was analyzed as in (Pekkurnaz et al., 2014). Briefly, we defined mitochondria as motile when the

Author Manuscript Author Manuscript Author Manuscript Author Manuscript

average of the instantaneous velocity was higher than 0.05μm/s (Wang and Schwarz, 2009). Mitochondria whose velocity was equal or lower than this threshold were considered as stationary. The moving frequency was defined as the percentage of time each mitochondrion spent in motion during the time of the recording and was calculated by dividing the time spent in motion by the total recording time. Hence, the motile pool of mitochondria were the mitochondria with a moving frequency higher than 0. The moving frequency of the motile mitochondria was calculated by excluding the stationary mitochondria. The moving frequency of individual mitochondria was used for statistical analysis. For the percentage of mitochondria in motion per axons, statistics were done on the number of axons. The density of mitochondria in axons was calculated by counting the number of mitochondria on the first frame of the recording used for mitochondrial transport analysis normalized by the length of the axons.

Surgical procedures

All experiments procedures were performed in compliance with animal protocols approved by the IACUC at Boston Children's Hospital. For all procedures, mice were anaesthetized with ketamine and pyrazine. Eye ointment containing atropine sulfate was applied to protect the cornea during surgery. Animals received Buprenorphine (0,05 mg/kg, Bedford lab) for 24 hours as post-operative analgesic. Surgical procedures were achieved as described in (Park et al., 2008). AAV virus injection: 1uL of AAV2 viruses were injected into the right eye of the different mice lines. A glass micropipette was inserted to peripheral retina, behind ora serrate in a way to avoid damage to the lens. When two viruses were injected, viruses were mixed and injected at the same time. The following viruses were used: AAV2-Cre, AAV2-PLAP, AAV2-Armcx1HA, AAV2-Armcx1HAΔTM, AAV2-CNTF, AAV2-shRNA Scramble and AAV2-shRNA Armcx1. The titers of the viruses were comprised between 10^{12} −10^{13}gc/mL. Viruses were produced at the Boston Children's Hospital viral core. Optic nerve injury: Four weeks following AAV2 injection (5 weeks for AAV-shRNAs), the right optic nerve was exposed intraorbitally and crushed with forceps (Dumont #5 FST) for 5 seconds approximately 1mm behind the eye ball. RGC anterograde labeling: 2-3 days before animals were euthanized, 1.5ul of cholera toxin β subunit (CTB-2ug/ul, in sterile PBS-Life Technologies) coupled with Alexa-555 (CTB-Alexa-555) was injected into the vitreous with Hamilton syringe (Hamilton) to label axons in optic nerve.

Axon regeneration imaging and quantification

Optic nerves cryo-sections of 14μm thick were imaged with a 20x objective using a PerkinElmer Spinning Disc confocal microscope equipped with a motorized stage and Volocity software (Perkin Elmer). For each nerve section, Z-projected to maximum intensity stacked images were stitched together with a 20% of overlap between each image to generate a single picture of the whole optic nerve. Regenerating axons were quantified as described in (Park et al., 2008). For whole mount optic nerve imaging, we followed the protocol described in (Pernet et al., 2013) with minor modifications. Briefly, optic nerves from perfused mice were post-fixed overnight washed three times 10mn in PBS and incubated at room temperature for 20 min in increasing concentration of ethanol (50%, 80%, 95%, 100%). Nerves were kept at 4°C overnight in ethanol 100% with constant agitation. Nerves were then put in Hexan (Sigma) for 3 hours at room temperature on a shaker. The

Author Manuscript Author Manuscript Author Manuscript Author Manuscript

clearing was completed by replacing Hexan by a solution of Benzyl alcohol/Benzyl Benzoate (1 : 2). Nerves were stored in the dark at room temperature in this final solution. For imaging, we used PerkinElmer Spinning Disc confocal microscope equipped with 20x objective and a motorized stage and Volocity software (Perkin Elmer). The whole nerve was acquired using optical sections of 2μm and stitched images of the Z stacks projections to maximum intensity.

RGC survival imaging and quantification

Whole mount retinas were immunostained with anti-Tuj1 antibody (Covance Research Products Inc Cat# MMS-435P, RRID:AB_2313773 or Covance Research Products Inc Cat# MRB-435P-100, RRID:AB_10175616). Because of the layering pattern of the retina with the RGCs layer sitting on the top of a whole mount preparation, Tuj1 staining efficiently labeled RGCs (Belin et al., 2015; Nawabi et al., 2015; Park et al., 2008; Smith et al., 2009). Pictures from 10 regions per retina were taken under an epifluorescence microscope (Nikon 80i-20X objective). Tuj1 positive RGCs were counted in intact and injured eye for each animal. The number of Tuj1 positive RGCs in intact eye of each animal was considered as 100% for this particular animal and was compared to its injured eye to quantify the survival.

Statistical Analysis

Statistical analysis was performed with GraphPad Prism v6.0. Normality tests were run to assess the distribution of the data to be statistically analyzed. Non normal distributions were analyzed using non-parametric test: Mann-Whitney U test was used to determine the significance of differences between two conditions and the Kruskal-Wallis nonparametric ANOVA test when multiple conditions were compared. Normal distributions were analyzed using parametric test: Student’s t-test was used to determine the significance of differences between two conditions and the one-way ANOVA test with Tuckey’s multiple comparison test unless otherwise specified. $p < 0.05$ was considered significant. For box plot graph, whiskers represent the maximum and minimum of the distribution and the horizontal bar in the box the median. For bar plots, all data are shown as mean +/− SEM.

Supplementary Material

Refer to Web version on PubMed Central for supplementary material.

Acknowledgments

We thank Dr. Homaira Nawabi for assistance with adult retina explant culture. Dr. Gulcin Pekkurnaz for discussion and valuable inputs. Drs. Phillipe Williams and Nahid Iglesias for critical reading of the manuscript. Lab members from Schwarz and He lab for technical advice. This study was supported by fellowships from International Foundation for Research in Paraplegia, Wings for Life Spinal Cord Research Foundation and Swiss National Science Foundation (RC), grants from R01EY021242 and Dr. Miriam and Sheldon G. Adelson Medical Research Foundation (ZH) and R01GM069808 (TLS). IDDRC and viral cores supported by the NIH grants P30 HD018655 and P30EY012196 were used for this study.

References

Abe N, Cavalli V. Nerve injury signaling. Current Opinion in Neurobiology. 2008; 18:276–283. [PubMed: 18655834]

Author Manuscript Author Manuscript Author Manuscript Author Manuscript

Bei F, Lee HHC, Liu X, Gunner G, Jin H, Ma L, Wang C, Hou L, Hensch TK, Frank E, et al. Restoration of Visual Function by Enhancing Conduction in Regenerated Axons. Cell. 164:219–232.

Belin S, Nawabi H, Wang C, Tang S, Latremoliere A, Warren P, Schorle H, Uncu C, Woolf CJ, He Z, et al. Injury-Induced Decline of Intrinsic Regenerative Ability Revealed by Quantitative Proteomics. Neuron. 2015; 86:1000–1014. [PubMed: 25937169]

Bonfanti L, Strettoi E, Chierzi S, Cenni MC, Liu XH, Martinou JC, Maffei L, Rabacchi SA. Protection of retinal ganglion cells from natural and axotomy-induced cell death in neonatal transgenic mice overexpressing bcl-2. J Neurosci. 1996; 16:4186–4194. [PubMed: 8753880]

Bradke F, Fawcett JW, Spira ME. Assembly of a new growth cone after axotomy: the precursor to axon regeneration. Nature Reviews Neuroscience. 2012; 13:183–193. [PubMed: 22334213]

Cartoni R, Léger B, Hock MB, Praz M, Crettenand A, Pich S, Ziltener J-L, Luthi F, Dériaz O, Zorzano A, et al. Mitofusins 1/2 and ERRalpha expression are increased in human skeletal muscle after physical exercise. The Journal of Physiology. 2005; 567:349–358. [PubMed: 15961417]

Courchet J, Lewis TL Jr. Lee S, Courchet V, Liou D-Y, Aizawa S, Polleux F. Terminal Axon Branching Is Regulated by the LKB1-NUAK1 Kinase Pathway via Presynaptic Mitochondrial Capture. Cell. 2013; 153:1510–1525. [PubMed: 23791179]

Cregg JM, DePaul MA, Filous AR, Lang BT, Tran A, Silver J. Functional regeneration beyond the glial scar. Experimental Neurology. 2014; 253:197–207. [PubMed: 24424280]

De Vos KJ, Grierson AJ, Ackerley S, Miller CCJ. Role of Axonal Transport in Neurodegenerative Diseases*. Annu. Rev. Neurosci. 2008; 31:151–173. [PubMed: 18558852]

Duan X, Krishnaswamy A, la Huerta, De I, Sanes JR. Type II cadherins guide assembly of a direction-selective retinal circuit. Cell. 2014; 158:793–807. [PubMed: 25126785]

Duan X, Qiao M, Bei F, Kim I-J, He Z, Sanes JR. Subtype-Specific Regeneration of Retinal Ganglion Cells following Axotomy: Effects of Osteopontin and mTOR Signaling. Neuron. 2015; 85:1244–1256. [PubMed: 25754821]

Glater EE, Megeath LJ, Stowers RS, Schwarz TL. Axonal transport of mitochondria requires milton to recruit kinesin heavy chain and is light chain independent. The Journal of Cell Biology. 2006; 173:545–557. [PubMed: 16717129]

Goldberg JL, Barres BA. The relationship between neuronal survival and regeneration. Annu. Rev. Neurosci. 2000; 23:579–612. [PubMed: 10845076]

Goldberg JL, Espinosa JS, Xu Y, Davidson N, Kovacs GTA, Barres BA. Retinal ganglion cells do not extend axons by default: promotion by neurotrophic signaling and electrical activity. Neuron. 2002; 33:689–702. [PubMed: 11879647]

Hammarlund M, Jin Y. Axon regeneration in C. elegans. Current Opinion in Neurobiology. 2014; 27:199–207. [PubMed: 24794753]

He Z, Jin Y. Intrinsic control of axon regeneration. Neuron. 2016; 90:437–451. [PubMed: 27151637]

Hinckelmann M-V, Zala D, Saudou F. Releasing the brake: restoring fast axonal transport in neurodegenerative disorders. Trends in Cell Biology. 2013

Hu Y, Park KK, Yang L, Wei X, Yang Q, Cho K-S, Thielen P, Lee A-H, Cartoni R, Glimcher LH, et al. Differential effects of unfolded protein response pathways on axon injury-induced death of retinal ganglion cells. Neuron. 2012; 73:445–452. [PubMed: 22325198]

López-Doménech G, Serrat R, Mirra S, D'Aniello S, Somorjai I, Abad A, Vitureira N, García-Arumí E, Alonso MT, Rodriguez-Prados M, et al. The Eutherian Armcx genes regulate mitochondrial trafficking in neurons and interact with Miro and Trak2. Nature Communications. 2012; 3:814.

Lu Y, Belin S, He Z. Signaling regulations of neuronal regenerative ability. Current Opinion in Neurobiology. 2014; 27:135–142. [PubMed: 24727245]

Mar FM, Simões AR, Leite S, Morgado MM, Santos TE, Rodrigo IS, Teixeira CA, Misgeld T, Sousa MM. CNS Axons Globally Increase Axonal Transport after Peripheral Conditioning. Journal of Neuroscience. 2014; 34:5965–5970. [PubMed: 24760855]

Martinou J-C, Dubois-Dauphin M, Staple JK, Rodriguez I, Frankowski H, Missotten M, Albertini P, Talabot D, Catsicas S, Pietra C. Overexpression of BCL-2 in transgenic mice protects neurons from naturally occurring cell death and experimental ischemia. Neuron. 1994; 13:1017–1030. [PubMed: 7946326]

Author Manuscript Author Manuscript Author Manuscript Author Manuscript

Misgeld T, Kerschensteiner M, Bareyre FM, Burgess RW, Lichtman JW. Imaging axonal transport of mitochondria in vivo. Nature Publishing Group. 2007; 4:559–561.

Morris RL, Hollenbeck PJ. The regulation of bidirectional mitochondrial transport is coordinated with axonal outgrowth. J Cell Sci. 1993; 104:917–927. Pt 3. [PubMed: 8314882]

Mou Z, Tapper AR, Gardner PD. The armadillo repeat-containing protein, ARMCX3, physically and functionally interacts with the developmental regulatory factor Sox10. Journal of Biological Chemistry. 2009; 284:13629–13640. [PubMed: 19304657]

Nawabi H, Briancon-Marjollet A, Clark C, Sanyas I, Takamatsu H, Okuno T, Kumanogoh A, Bozon M, Takeshima K, Yoshida Y, et al. A midline switch of receptor processing regulates commissural axon guidance in vertebrates. Genes & Development. 2010; 24:396–410. [PubMed: 20159958]

Nawabi H, Belin S, Cartoni R, Williams PR, Wang C, Latremoliere A, Wang X, Zhu J, Taub DG, Fu X, et al. Doublecortin-Like Kinases Promote Neuronal Survival and Induce Growth Cone Reformation via Distinct Mechanisms. Neuron. 2015

Park KK, Liu K, Hu Y, Smith PD, Wang C, Cai B, Xu B, Connolly L, Kramvis I, Sahin M, et al. Promoting axon regeneration in the adult CNS by modulation of the PTEN/mTOR pathway. Science. 2008; 322:963–966. [PubMed: 18988856]

Pekkurnaz G, Trinidad JC, Wang X, Kong D, Schwarz TL. Glucose Regulates Mitochondrial Motility via Milton Modification by O-GlcNAc Transferase. Cell. 2014; 158:54–68. [PubMed: 24995978]

Pernet V, Joly S, Jordi N, Dalkara D, Guzik-Kornacka A, Flannery JG, Schwab ME. Misguidance and modulation of axonal regeneration by Stat3 and Rho/ROCK signaling in the transparent optic nerve. Cell Death Dis. 2013; 4:e734. [PubMed: 23868067]

Sanes JR, Masland RH. The types of retinal ganglion cells: current status and implications for neuronal classification. Annu. Rev. Neurosci. 2015

Schwarz TL. Mitochondrial trafficking in neurons. Cold Spring Harb Perspect Biol. 2013; 5

Smith P, Sun F, Park KK, Cai B, Wang C, Kuwako K, Martinez-Carrasco I, Connolly L, He Z. SOCS3 deletion promotes optic nerve regeneration in vivo. Neuron. 2009; 64:617–623. [PubMed: 20005819]

Song J, Giang A, Lu Y, Pang S, Chiu R. Multiple shRNA expressing vector enhances efficiency of gene silencing. BMB Rep. 2008; 41:358–362. [PubMed: 18510865]

Sun F, Park KK, Belin S, Wang D, Lu T, Chen G, Zhang K, Yeung C, Feng G, Yankner BA, et al. Sustained axon regeneration induced by co-deletion of PTEN and SOCS3. Nature. 2012; 480:372–375.

Trushina E, Nemutlu E, Zhang S, Christensen T, Camp J, Mesa J, Siddiqui A, Tamura Y, Sesaki H, Wengenack TM, et al. Defects in mitochondrial dynamics and metabolomic signatures of evolving energetic stress in mouse models of familial Alzheimer's disease. PLoS ONE. 2012; 7:e32737. [PubMed: 22393443]

Verburg J, Hollenbeck PJ. Mitochondrial Membrane Potential in Axons Increases with Local Nerve Growth Factor or Semaphorin Signaling. Journal of Neuroscience. 2008; 28:8306–8315. [PubMed: 18701693]

Wang X, Schwarz TL. The Mechanism of Ca. Cell. 2009; 136:163–174. [PubMed: 19135897]

Wang X, Winter D, Ashrafi G, Schlehe J, Wong YL, Selkoe D, Rice S, Steen J, LaVoie MJ, Schwarz TL. PINK1 and Parkin Target Mirofor Phosphorylation and Degradation to Arrest Mitochondrial Motility. Cell. 2011; 147:893–906. [PubMed: 22078885]

Wernet MF, Huberman AD, Desplan C. So many pieces, one puzzle: cell type specification and visual circuitry in flies and mice. Genes & Development. 2014; 28:2565–2584. [PubMed: 25452270]

Zhang L, Trushin S, Christensen TA, Bachmeier BV, Gateno B, Schroeder A, Yao J, Itoh K, Sesaki H, Poon WW, et al. Altered brain energetics induces mitochondrial fission arrest in Alzheimer's Disease. Sci. Rep. 2016; 6:18725. [PubMed: 26729583]

Zhou B, Yu P, Lin M-Y, Sun T, Chen Y, Sheng Z-H. Facilitation of axon regeneration by enhancing mitochondrial transport and rescuing energy deficits. J Cell Biol. 2016; 104 jcb.201605101.

Zukor K, Belin S, Wang C, Keelan N, Wang X, He Z. Short hairpin RNA against PTEN enhances regenerative growth of corticospinal tract axons after spinal cord injury. - PubMed - NCBI. J Neurosci. 2013; 33:15350–15361.

Author Manuscript Author Manuscript Author Manuscript Author Manuscript

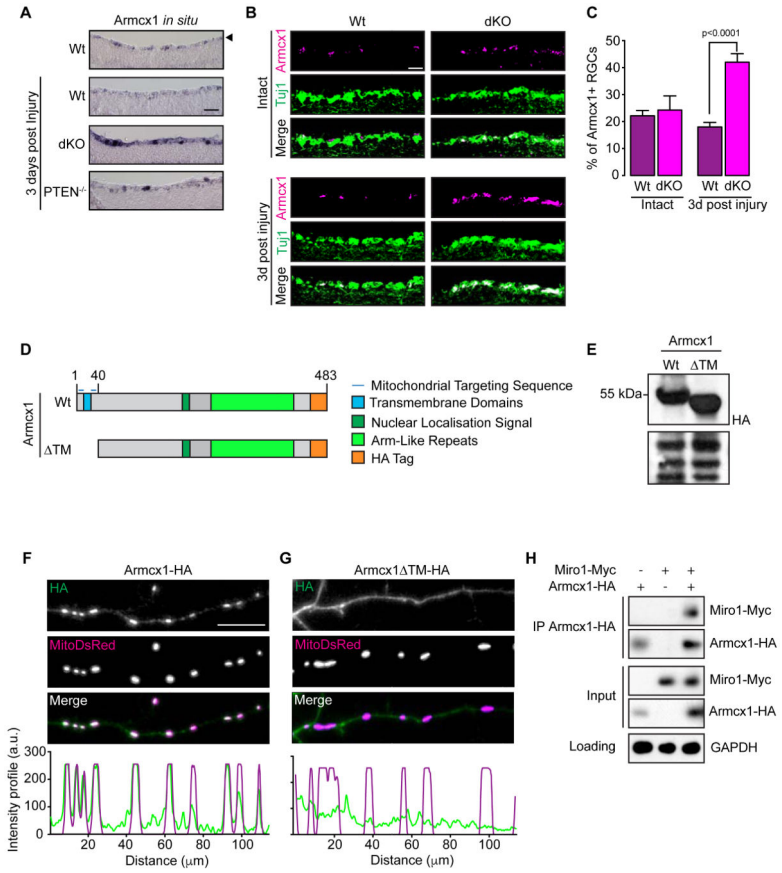

Figure 1. Armcx1 is up-regulated in high regeneration conditions in vivo and localizes to mitochondria

(A) In situ hybridization showing Armcx1 mRNA levels in mouse retina cross-sections of wild type and high regeneration mutant PTEN, SOCS3 double KO +CNTF (dKO) and PTEN single KO ($PTEN^{-/-}$) in intact conditions or 3 days post optic nerve crush. Arrow head indicates the retinal ganglion cells layer (GCL). Scale bar: 50μm. (B) Immunohistochemistry showing the level of endogenous Armcx1 protein in intact retina or 3 days post optic nerve crush in wild type and high regeneration mutant dKO. Tuj1 antibody is used as a RGC marker. Scale bar: 50μm. (C) Quantification of the percentage of Armcx1 positive RGCs from matched sections of 2-3 animals per condition. One-way ANOVA with Tuckey's multiple comparison test. (D) Scheme of Armcx1 constructs full length and mutant. (E) Immunoblot using anti-HA antibody on HEK cell extract transfected either with Armcx1-HA full length or Armcx1-HA lacking the trans membrane domain (Armcx1ΔTM-HA). Lower panel shows unspecific bands of lower molecular weights used as loading control. (F-G) Immunohistochemistry using anti-HA antibody of mouse cortical neurons co-transfected with MitoDsRed2 and Armcx1-HA (F) or Armcx1ΔTM-HA (G). Low magnification picture of transfected neurons can be seen in Supp. Fig. 1B. Lower panel shows signal intensity measured by line scan. Scale bar: 25μm. (H) Representative immunoblot showing the specific co-immunoprecipitation (IP) of Miro1-Myc with Armcx1-HA in HEK cells (n=3).

Author Manuscript Author Manuscript Author Manuscript Author Manuscript

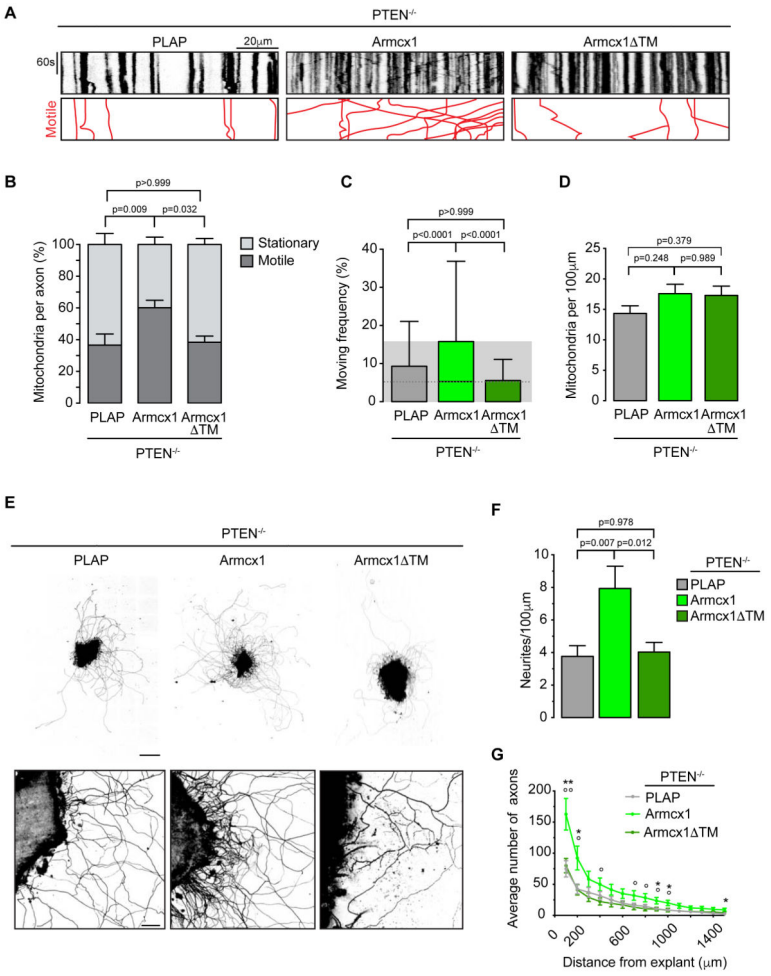

Figure 2. Armcx1 increases mitochondrial transport and axonal outgrowth of adult RGCs

(A) Representative kymographs from live imaging of TMRM labeled mitochondria in RGC axons of adult retina explant from PTEN$^{f/f}$ mice co-injected with AAV-Cre and either AAV-PLAP, AAV-Armcx1 or AAV-Armcx1ΔTM. (B) Percentage of motile and stationary mitochondria in adult RGC axons of the indicated genotypes. n=12-17 axons from 3 independent experiments. Kruskal-Wallis test with Dunn's multiple comparisons test on the number of axons. (C) Box plot showing the moving frequency of mitochondria in RGC axons of adult retina explants from the indicated genotypes. n=221-348 mitochondria from 3 independent experiments (11-16 axons). Kruskal-Wallis test with Dunn's multiple comparisons test (D) Mitochondrial density in adult RGCs axons. n=11-16 axons from 3 independent experiments. One-way ANOVA with Tuckey's multiple comparisons test. (E) Tuj1 immunostaining of explants of the indicated genotype. Scale bar: 500µm (upper row) and 100µm (lower row). (F) Quantification of the number of axons growing out of the explant normalized by explant's size. n=14-16 explants (21-182 axons) from 2 independent experiments. One-way ANOVA with Tuckey's multiple comparisons test. (G) Quantification of the axonal outgrowth for explants of the indicated genotypes. n=14-16 explants from 2 independent experiments. PTEN$^{-/-}$ +Armcx1 vs PTEN$^{-/-}$ +PLAP: *p < 0.05 and **p <

Author Manuscript Author Manuscript Author Manuscript Author Manuscript

0.01. PTEN$^{-/-}$ +Armcx1 vs PTEN$^{-/-}$ +ARMCX1ΔTM: °$p < 0.05$ and °°$p < 0.01$. One-way ANOVA with Tuckey's multiple comparisons test.

Author Manuscript Author Manuscript Author Manuscript Author Manuscript

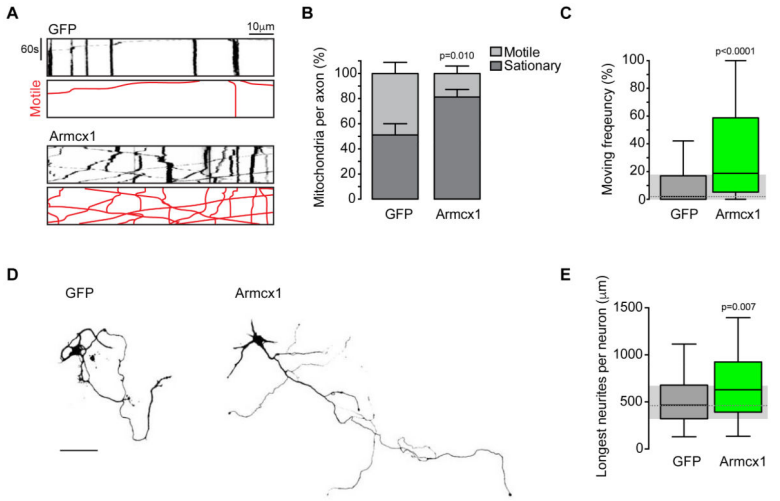

Figure 3. Effect of Armcx1 overexpression in E18 cortical neurons

(A) Representative kymographs from live imaging of mitochondria in E18 cortical neurons co-transfected with MitoDsRed and either GFP or Armcx1-F2A-GFP. Traces from motile mitochondria were isolated and represented bellow kymographs. (B) Percentage of motile and stationary mitochondria per axon of E18 cortical neurons transfected as in A. n=8-10 axons from 3 independent experiments. Two tailed Student's Unpaired t-test on the number of axons. (C) Box plot showing the moving frequency (percentage of time each mitochondria in motion) of mitochondria in axons from cortical neurons of the indicated genotypes. The horizontal line shows the median of the distribution. n=74-137 mitochondria from 3 independent experiments (8-10 axons). Mann-Whitney U test. (D) Representative images of E18 cortical neurons transfected with GFP or Armcx1-F2A-GFP. Scale bar: 100µm. (E) Box plots showing the distribution of the measurements of the longest neurite in E18 cortical neurons transfected as in (D). N=54-97 neurons from 3 independent experiments ran in duplicate. Mann-Whitney U test.

Author Manuscript Author Manuscript Author Manuscript Author Manuscript

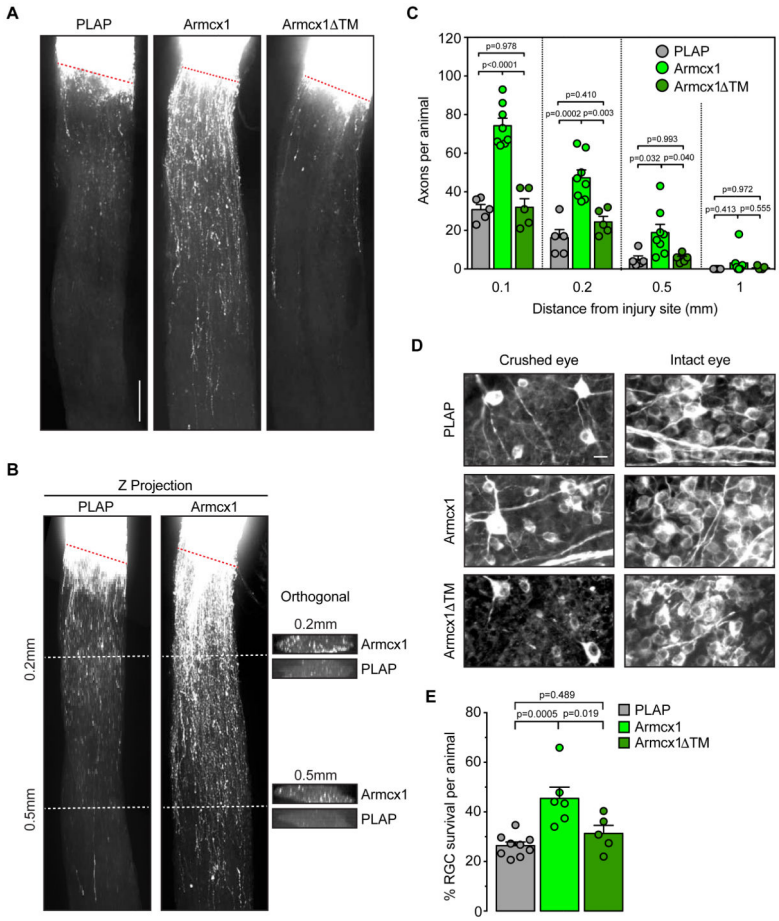

Figure 4. Armcx1 promotes axonal regeneration and neuronal survival

(A) Optical sections (approximately 14μm) from whole mount cleared optic nerve from wild type mice injected with AAV -PLAP, AAV-Armcx1 or AAV-Armcx1ΔTM, 15 days post optic nerve crush (dashed red line). Axons were labeled with CTB injection. Scale bar: 100μm. (B) Full nerve thickness z projections of the cleared optic nerves shown in A. (C) Bar plot showing the average total number of axons growing past the injury site based on the z projection of the whole mount cleared optic nerve. Each dot represents one mouse. n=5-8 mice from 2 independent experiments. One-way ANOVA, Tuckey's multiple comparison test. (D) Tuj1 immunohistochemistry on whole mount retina from wild type mice shown in A. The retina from the crushed eye (right) and intact eye (left) of the same animal is shown. Scale bar: 40μm. (E) Average percentage of RGC survival as measured by Tuj1 staining. Each dot represents one animal. N = 5-9 mice from two independent experiments. One-way ANOVA, Tuckey's multiple comparison test.

Author Manuscript Author Manuscript Author Manuscript Author Manuscript

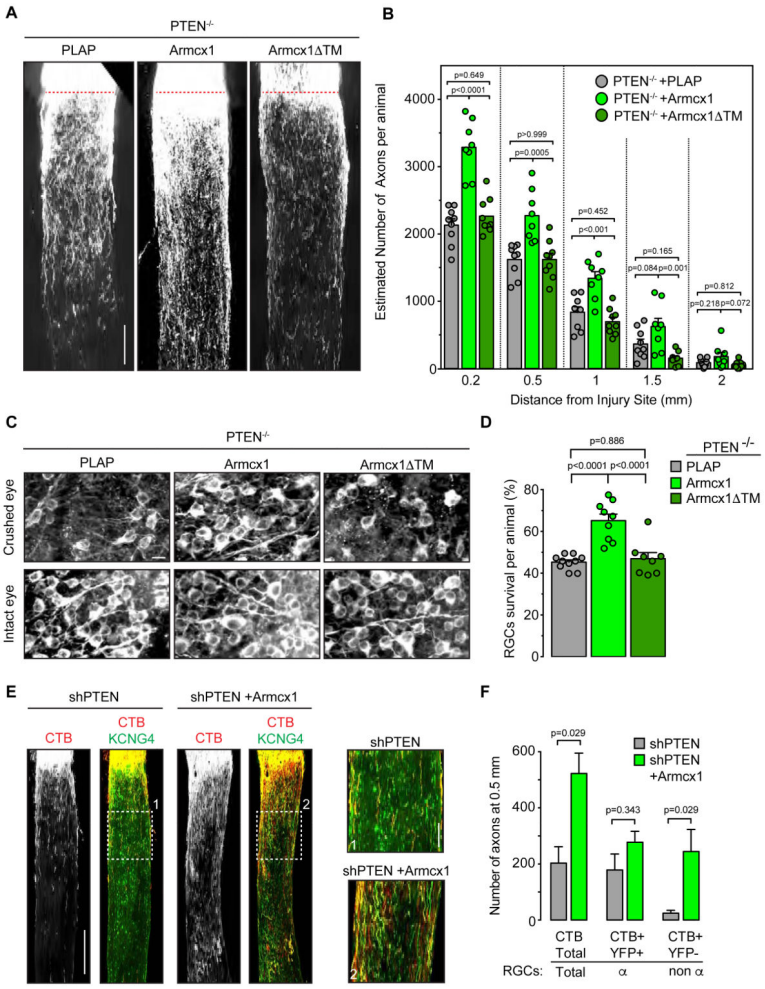

Figure 5. Armcx1 potentiates axonal regeneration of PTEN deleted RGCs

(A) Optic nerve sections of PTEN$^{f/f}$ mice co-injected with AAV-Cre and the indicated AAVs, 15 days post optic nerve crush (dashed red line). Axons were labeled with intraocular CTB injection. Scale bar: 100μm. Pictures of the full nerve can be seen in figure S5. (B) Bar plot showing the average estimated number of axons growing past the injury site. Each dot represents one animal (2-6 cryo-sections per animal). n=8-9 mice from 2 independent experiments. One-way ANOVA, Tuckey's multiple comparison test. (C) Tuj1 immunohistochemistry of whole mount retina from PTEN$^{f/f}$ mice shown in A. Retina from the crushed eye (right) and intact eye (left) of the same animal is shown. Scale bar: 40μm. (D) Average percentage of RGC survival per animal measured by Tuj1 staining. Each dot represents one animal. n=8-9 animals. One-way ANOVA, Tuckey's multiple comparison test. Scale bar: 40μm. (E) Optic nerve longitudinal sections 15 days post crush of Kcng4-YFP mice injected with CTB and the indicated AAVs. The YFP channel (green) shows the axons projecting from the αRGCs (Kcng4-YFP) and the RFP channel (red) shows the CTB labeled axons from all RGCs. (F) CTB and YFP axons quantified 0.5 mm from the injury site. n=4 mice per condition. Mann-Whitney U test. Scale bar: 300μm.

Author Manuscript Author Manuscript Author Manuscript Author Manuscript

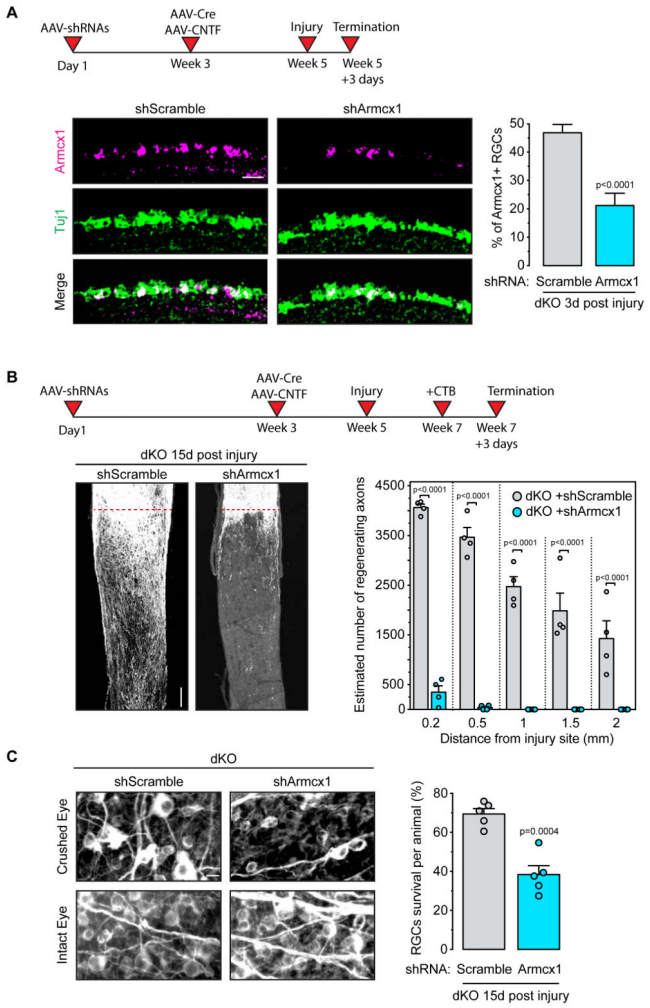

Figure 6. Armcx1 is necessary for axonal regeneration

(A) Experimental timeline and (left) immunohistochemistry using Armcx1 antibody on retina cross sections of dKO mice injected either with AAV-shScramble or AAV-shArmcx1. Mice were euthanized 3 days post optic nerve crush. (Right) Quantification of the number of Armcx1 positive RGCs 3 days post optic nerve crush in matching sections of the indicated genotypes. Scale bar: 40μm. n=3 mice randomly chosen from the cohort shown in (B). Two tailed Student's Unpaired t-test. (B) Experimental timeline and (left) optic nerve sections of dKO mice injected with indicated AAVs, 15 days post optic nerve crush (dashed red line). Axons were labeled with CTB injection. Scale bar: 100μm. Pictures of the full nerve are shown in figure S6I. (Right) Bar plot showing the average estimated number of axons growing past the injury site per animal. Each dot represents one animal (2-6 cryo-sections per mice). n=4 per condition. One-way ANOVA, Tuckey's multiple comparison test. (C) (Left) Tuj1 immunohistochemistry on whole mount retina from dKO mice injected with AAVs as shown in B. Retina from the crushed eye (upper) and intact eye (lower) of the same animal is shown. Scale bar: 40μm. (Right) Bar plot of the average percentage of RGC survival per animal measured by Tuj1 staining. Each dot represents one animal. N=5 per condition. Two tailed Student's Unpaired t-test.